HHS Public Access

Author manuscript

J Comput Aided Mol Des. Author manuscript; available in PMC 2020 January 01.

Published in final edited form as:

J Comput Aided Mol Des. 2019 January ; 33(1): 105–117. doi:10.1007/s10822-018-0162-6.

Calculate Protein-Ligand Binding Affinities with the Extended Linear Interaction Energy Method: Application on the Cathepsin S Set in the D3R Grand Challenge 3

Xibing HE[1], **Viet H. MAN**[1], **Beihong JI**[1], **Xiang-Qun XIE**[1], and **Junmei WANG**[1,*]

[1]Department of Pharmaceutical Sciences and Computational Chemical Genomics Screening Center, School of Pharmacy, University of Pittsburgh, Pittsburgh, Pennsylvania 15261, United States

Abstract

We participated the Cathepsin S (CatS) sub-challenge of the Drug Design Data Resource (D3R) Grand Challenge 3 (GC3) in 2017 to blindly predict the binding poses of 24 CatS-bound ligands, the binding affinity ranking of 136 ligands, and the binding free energies of a subset of 33 ligands in Stage 1A & Stage 2. Our submitted predictions ranked relatively well compared to the submissions from other participants. Here we present our methodologies used in the challenge. For the binding pose prediction, we employed the Glide module in the Schrodinger Suite 2017 and AutoDock Vina. For the binding affinity / free energy prediction, we carried out molecular dynamics (MD) simulations of the complexes in explicit water solvent with counter ions, and then estimated the binding free energies with our newly developed model of Extended Linear Interaction Energy (ELIE), which is inspired by two other popular end-point approaches: the Linear Interaction Energy (LIE) method, and the Molecular Mechanics with Poisson-Boltzmann Surface Area solvation (MM/PBSA) method. Our studies suggest that ELIE is a good trade-off between efficiency and accuracy, and it is appropriate for filling the gap between the high-throughput Docking & Scoring methods and the rigorous but much more computationally demanding methods like free energy perturbation (FEP) or thermodynamics integration (TI) in computer-aided drug design (CCAD) projects.

Keywords

MM/GBSA; alchemical free energy calculations; binding mode; binding affinity; virtual screening; lead identification; lead optimization

[*]Corresponding author: Dr. Junmei WANG, juw79@pitt.edu.

Supporting Information. Supplementary Material is provided with this manuscript. Figure S1, 2D structures of the the tetrahydropyrido-pyrazole core and the pyridinone-like core in the Cathepsin S ligands. Figure S2, 2D structure of CatS-5. Figure S3, Performance of ranking predictions in Stage 2 of CatS set. Figure S4, Performance of submissions for the CatS Free Energy set in Stage 2.

Introduction

Drug Design Data Resource (D3R) [1] is an NIH founded organization based at the University of California San Diego (UCSD). D3R collects high-quality, unpublished crystal structures and affinity data of protein-ligand binding complexes donated by pharmaceutical companies, and uses these data to organize challenges of blind prediction of ligand binding poses and protein-ligand binding affinities [2, 3]. The purposes of such blind prediction challenges are to test the state-of-the-art computational methodologies and protocols in the field of computer-aided drug design/discovery (CADD), and advance the development of CADD technologies. The D3R Grand Challenge 3 (GC3) was held from Aug. 31st 2017 to Dec 15th 2017 and involved 5 subchallenges: *Subchallenge 1* Cathepsin S; *Subchallenge 2* Kinase Selectivity; *Subchallenge 3* Kinase Activity Cliff JAK2_SC3; *Subchallenge 4* Kinase Activity Cliff TIE2; *Subchallenge 5* Kinase Mutants [4]. Participants from the computational chemistry community worldwide were asked to complete the subchallenges in the order they were listed, i.e., to complete the *Subchallenge 1* first if the time and resource were limited, then complete *Subchallenge 2* if their time and resource were allowed, and so on. We only participated in the *Subchallenge 1* (the Cathepsin S set) due to limited computing resource.

The cathepsins are a very important family of cysteine proteases in humans. They are in various functions, such as bulk intracellular proteolysis in the endolysosomal system, cell death and inflammation signaling in the cytoplasm, cell-cycle regulation in the nucleus, signaling in the extracellular environment, etc [5–8]. They are involved in a wide range of diseases such as cancers, chronic inflammation, infections, cardiovas-cular, and bone-related diseases [5–8]. Therefore, they have been investigated as drug targets for more than 2 decades by pharmaceutical companies and academic institutions. There are 11 sub-types of cathepsins: B, C, F, H, K, L, O, S, V, W, and X [5, 6]. Among these sub-types, the cathepsin S (CatS) has drawn special attentions, and its unique roles in the following diseases have been heavily investigated: rheumatoid arthritis, atherosclerosis, bronchial asthma, psoriasis, wound healing, myasthenia gravis, cancer, etc [7–18].

The data set of *Subchallenge 1* of GC3 was composed of 141 CatS ligands, among which 24 ligands had the protein-ligand co-crystallized structures determined with resolution < 3.0 Å, and 136 ligands had their bio-assay data (IC_{50}) measured [4]. However, all of the 24 crystal structures were not revealed at the beginning of the challenge, and all of the binding affinity data were blinded during the whole challenge time. This subchallenge was split into in 3 stages. In ***Stage 1A*** (Aug. 31st 2017 to Oct. 3rd 2017), participants were invited to: (a) predict the crystallographic poses of 24 ligands (the Binding Pose Set), (b) predict the affinity ranking of 136 ligands (the Affinity Ranking Set), and (c) predict the absolute or relative binding affinities for a subset of 33 compounds (the Free Energy Set). After ***Stage 1A*** was done, the pseudo-apo crystal structures of 24 complexes (with corresponding ligand coordinates removed) were released, and participants were invited to re-predict the binding poses of the 24 ligands in their own corresponding receptor structures (Self-Docking). No affinity calculations were involved in this stage called ***Stage IB*** (Oct. 9th, 2017 – Oct. 23rd, 2017). In the last stage, ***Stage 2*** (Oct. 24th, 2017 – Dec. 15th, 2017), full coordinates of the 24 protein-ligand co-crystal structures were released and participants were invited to re-

calculate the binding affinities for the Ranking Set & Free Energy Set, with or without usage of the 24 released crystal structures.

Our group participated the three predictions in ***Stage 1A*** and two predictions in ***Stage 2***, but did not participate in the Self-Docking ***Stage IB.*** According to the evaluation results done by the GC3 organizers in terms of root-mean-squared-deviations (RMSD) for pose predictions, correlations coefficients (Kendall's τ and Spearman's ρ) and root-mean-squared-errors (RMSE) for affinity predictions [19], our performances were relatively well compared to most of the other participants.

In the next section, we provide a detailed description of the methods and protocols which we employed for the predictions of binding poses and affinities of CatS subchallenge in D3R GC3. Especially, we focus on a new model named the Extended Linear Interaction Energy (ELIE) method, which were developed during our participating time in GC3. Then we present the results of applying the ELIE method to the CatS subchallenge in GC3, and discuss the advantages, shortcomings and future research plans with respect to the ELIE method.

Computational Methods

Theory Background

It has become a consensus that many docking methods can successfully predict near-native binding poses (position, conformation and orientation) of drug-like molecules in macromolecular receptors, but the corresponding scoring functions have poor abilities of estimating the binding free energies [2, 3], due to the usage of only static conformations of the receptor protein in prior docking procedures. On the other end, physics-based alchemical free energy calculation methods apply molecular dynamics (MD) or Monte Carlo (MC) simulations to sample the dynamic conformations of the receptor, the ligand and the complex in explicit solvent, and can accurately describe the flexibilities of receptor-ligand binding and the solution. The free energy perturbation (FEP) and thermodynamic integration (TI) are examples of such rigorous methods [20–25]. For instance, the FEP+ protocol implemented by Schrodinger Inc. (USA) have become the *de facto* standard metric for industrial drug modeling practice [22]. However, FEP and TI need to run on a series of unphysical intermediate states along the pathways of alchemical changes. The slow convergence problem and extensive sampling needed make FEP/TI too computationally demanding to be routinely used in real drug design projects. Consequently, some approximate end-point methods such as linear interaction energy (LIE) [26–29], molecular mechanics (MM) combined with Poisson–Boltzmann (PB) or generalized Born (GB) and surface area (SA) continuum solvation (MM/PBSA or MM/GBSA), have been developed [30–32]. They are in the intermediate position in terms of efficiency and accuracy between empirical scoring functions and the FEP/TI methods.

The LIE approach estimate the binding free energy according to the following equation:

$$\Delta G_{bind}^{LIE} = \alpha\left(\left\langle U_{elec}^{L-S}\right\rangle_{PL} - \left\langle U_{elec}^{L-S}\right\rangle_{L}\right) + \beta\left(\left\langle U_{vdw}^{L-S}\right\rangle_{PL} - \left\langle U_{vdw}^{L-S}\right\rangle_{L}\right) + \gamma \quad (1)$$

where the subscripts PL and L indicate two states on which the MD/MC simulations are running: the state of protein-ligand complex in solution (PL), and the state of ligand free in solution (L), correspondingly. The < > brackets indicate ensemble averages from MD/MC simulations. The superscript L-S indicates that the LIE approach only considers the interactions between the ligand and the surroundings (S), which refers to protein and solution in the PL state, and solution only in the L state. The scale factor α was originally set as 0.5 according to the linear-response approximation (LRA), and β is taken to be 0.18. Later α was treat as adjustable between 0.33 and 0.5, depending on the charge and number of hydrogen-bond (H-bond) donors of the ligand [26–29]. In many later applications, different α and β values were adjusted and adopted to get better results. An optional constant γ can also be added to improve the estimations.

The MM/PBSA and MM/GBSA methods calculate a free energy from:

$$\Delta G = \Delta E_{inter} + \Delta E_{elec} + \Delta E_{vdw} + \Delta G_{solv\_pl} + \Delta G_{solv\_np} - T\Delta S \quad (2)$$

where ΔE_{inter} is the change of internal bonded MM energy from the bonds, angles and torsions/dihedrals, ΔE_{elec} is the change of MM electrostatic energy, ΔE_{vdw} is the change of MM van der Waals energy, ΔG_{slov_pl} is the polar solvation free energy, ΔG_{solv_up} is the nonpolar solvation free energy, T is the absolute temperature, and ΔS is the entropy change. ΔG_{solv_pl} can be calculated by any continuum-solvation method such as PB or GB. $\Delta Gsolv_{\_np}$ is obtained from a linear relation to the solvent-accesssible surface area (SASA). The entropic contributions can be estimated from normal-mode analysis on a set of conformational snapshots obtained from MD/MC simulations.

In principle the binding free energy in Eq. 2 should be computed from the differences in PL, P and L states. But in real application, a much more common approach is to simulate only PL complex state, whereas the P or L conformations are approximated by simply removing other particles and only keeping the protein or ligand coordinates, respectively. This approach not only require fewer simulations, but also leads to an exact cancellation of ΔE_{inter}. Hence,

$$\Delta G = \Delta E_{elec} + \Delta E_{vdw} + \Delta G_{solv\_pl} + \Delta G_{solv\_np} - T\Delta S \quad (3)$$

The LIE approach only considers contributions from the electrostatic and van der Waals interaction energies, and scale them by fitted coefficients. The MM/PBSA method considers contributions not only from the electrostatic and van der Waals interaction energies but also from the polar and nonpolar contributions of solvation, but no scale factors are applied to these terms. Inspired by both the LIE and the MM/PBSA methods, we developed a new method to estimate the binding free energies of protein-ligand complexes, which we named

as the Extended Linear Interaction Energy (ELIE) method. In our ELIE approach, different scale coefficients are applied to each of energy terms in the MM/PBSA free energy equation (Eq. 3):

$$\Delta G = c0 + c1 * \Delta E_{elec} + c2 * \Delta E_{vdw} + c3 * \Delta G_{solv\_pl} + c4 * \Delta G_{solv\_np} - c5 * T\Delta S \quad (4)$$

where c0, c1, c2, c3, c4 & c5 are scaling coefficients, which need to be adjusted by fitting calculated binding free energies to measured values of ligands in the training set. Once optimum values are obtained for these scaling coefficients, they can be used to test sets to predict the binding free energies. The target receptor in the training set should be the same as in the test set.

Protein Preparation

At the beginning of ***Stage 1A***, D3R provided two crystal structures of pseudo-apo CatS, in which the originally bound ligands were removed. We conducted literature search and retrieved co-crystal structures for CatS from the RCSB Protein Data Bank [33], and found 20 holo structures of CatS bound with different ligands (PDB IDs: *1MS6, 1NPZ, 1NQC, 2F1G, 2H7J, 2HHN, 2HXZ, 2OP3, 2R9M, 2R9N, 2R9O, 3IEJ, 3KWN, 3MPE, 3MPF, 3N3G, 3N4C, 3OVX, 4P6E* AND *4P6G).* Among these holo proteins, ***3IEJ*** is particularly interesting because its ligand has a tetrahydropyrido-pyrazole core which is similar to the ligands in the Challenge Set, and this crystal structure has a good resolution of 2.18 Å [10]. Therefore, we decided to use it as starting point for Glide docking and MD simulations. The choice was also validated by the fact that the CαRMSDs between the two pseudo-apo CatS crystal structures provided by D3R and ***3IEJ*** are very low (0.35 Å).

After D3R released all 24 crystal structures in the CatS challenge set at the end of ***Stage 1B***, we aligned them to ***3IEJ*** and measured the CαRMSDs. All of the newly released crystal structures of CatS have very low CαRMSDs compared to ***3IEJ.*** The CatS-14 complex (structure code ***GABJ)*** has the largest CαRMSD (0.39 Å). We took ***GABJ*** as another starting point and repeated the procedures of MD simulations and binding affinity calculations with the ELIE model.

Selected crystal structures, including ***3IEJ*** from Protein Data Bank, CatS_SO4_structure_D3R_GC3.pdb provided by organizers at the beginning of ***Stage 1A*** gabj-CatS.pdb provided by organizers after ***Stage 1B***, were prepared using the Protein Preparation Wizard [34] in Maestro [35]. Missing hydrogen atoms were added. Missing side chains were filled using Prime [36]. All ionizable residues were assigned their protonation states using Epik [37] assuming a pH of 5.0, which was employed in the binding assay [18]. All crystallographic water and ions were removed. In order to avoid steric clashes, hydrogens of remaining protein (with or without ligand) structures were minimized using OPLS3 force field [38] while the heavy atoms were restrained using an RMSD cutoff of 0.3 Å.

Ligand Preparation

For the CatS subchallenge in GC3, D3R organizers provided participants with SMILES strings of 141 ligands, among which 24 ligands (from CatS_1 to CatS_24) have co-crystal structures, and 136 ligands have measured IC_{50} data between 3 to 8500 nM. These ligand molecules are referred as the Challenge Set in this article.

Most of the Challenge Set ligands share a common core scaffold of tetrahydropyrido-pyrazole, except for two ligands (CatS_4 and CatS_6) which have a pyridinone-like core (Figure S1 in Support Information). Through literature search, we collected structure information of approximately 130 ligands which also have a tetrahydropyrido-pyrazole core scaffold and which have corresponding IC_{50} data experimentally measured [9–13]. These ligand molecules are referred as the Training Set in this article.

The 3D structures of all ligands in both the Training and Challenge Sets were constructed by manually modifying the native ligand of a crystal structure (PDB ID ***3IEJ)*** [10]. Ligand protonation states were manually assigned. According to the reference [18] listed by the D3R organizer, the bio-assay measurements were performed at pH = 5.0 [18]. Therefore, we protonated all nitrogen atoms which are not in or connected to a double bond or aromatic bond. As a consequence, all of the ligand molecules have +1 or +2 net charges. The ligands were geometrically optimized in vacuum by Maestro using OPLS3 force-field [38]. The stereochemistry in all ligands were visually inspected against the descriptions in the provided SMILES strings for the Challenge Set or in the literature for the Training Set [9–13].

Pose prediction

Two docking approaches were used: Glide XP (extended precision) [39, 40], and AutoDock Vina [41]

For the Glide XP method, the prepared X-ray structure from PDB ID ***3IEJ*** was selected as the receptor template, because its co-crystallized ligand has the same scaffold core as in most of the challenge set, and it has a very low CαRMSD compared to the two pseudo-apo CatS crystal structures provided by D3R. Glide grid was generated with default options: van der Waals radius scaling factor 1.0, partial charge cutoff 0.25, centroid of workspace ligand, dock ligands similar in size to the workspace ligand, no constraints, no rotatable groups. The 3D ligand conformations as prepared above were used as the starting geometries. Each of the 24 ligands was docked against the same grid, using extra-precision (XP) sampling, reward intramolecular hydrogen bonds, post-docking minimization, and outputting a maximum of 5 poses per docking. All poses were ranked using Glide's XP docking scoring function. The best docking pose for each ligand was selected and submitted as our pose prediction.

The open source docking program Autodock Vina (version 1.1) was also employed. The CatS_SO4_structure_D3R_GC3.pdb provided by organizers was used as the receptor template. To prepare the input structures for the docking, the 3D structures in mol2 format of the 136 ligands were generated by Maestro from their SMILES format with considering all possible protonation and chirality. The MGLTools 1.5.4 was used to prepare the PDBQT

files for the receptor and ligands [42]. The dimensions of the docking rectangular box were 37 Å × 50 Å × 40 Å, to make sure the minimum distance between any atoms of the aligned ligands in the aforementioned 20 known co-crystallized CatS complexes to the box's walls is larger than 8 Å. The "exhaustiveness" of the global search was set 150 which is approximately 18 times larger than the default value 8, in order to increase the probability of finding the global minimum. Twenty binding modes were generated with random starting positions of each ligand, which had fully flexible torsion degrees of freedom. The maximum energy difference between the best and the worst binding modes was set 7.0 kcal/mol.

MD Simulation.

The Antechamber tool [43] integrated in AmberTools16 was utilized to generate topologies for use in MD. The protein-ligand complexes were all solvated in a cubic box with water extending at least 10 A from the complexes. Each system was neutralized adding Na^+ /Cl^- ions to a final concentration of 0.15 M. Disulfide bonds in CatS were specified.

Atom types and parameters for ligands were assigned by the General Amber force field (GAFF) [44]. The partial charges for ligands were derived using the AM1-BCC method [45], which was developed to resemble the partial charges derived by the restrained electrostatic potential (RESP) method [46] to fit the HF/6-31G* electrostatic potential generated using the GAUSSIAN 16 software package [47]. The ff14SB force-field [48] was adopted for CatS. Water molecules were treated with TIP3P water model [49].

The MD simulations were carried out using the PMEMD.mpi and PMEMD.cuda modules in the AMBER16 package [50–52]. A set of 5 steps of energy minimization were performed to remove possible steric crashes, first on water and ions, followed with the protein and ligand complex. The harmonic restraint force constants decreased from 20 to 10, 5, 1 and 0 kcal/mol/$Å^2$, progressively. After the minimization stages, each system was gradually heated from 0 K to 300 K and then the temperature was kept at 300 K. The time step of 1 fs was used for the heating and first part of equilibrium stage, then a 2 fs time step for the rest part of equilibrium and following production stages. The periodic boundary condition was employed to produce a constant temperature and pressure (NPT) ensemble. The pressure was controlled at 1 atm with a pressure relaxation time of 1 ps. The temperature was regulated using Langevin dynamics [53, 54] with a collision frequency of 5 ps^{-1}. The Particle Mesh Ewald (PME) method [55, 56] was adopted to handle the long-range electrostatics and a 10 Å cutoff was set to treat real-space interactions. All of the covalent bonds involving hydrogen atoms were constrained with the SHAKE algorithm [57]. The simulation time for each system was 10 ns. The first 5 ns was treated as equilibration and the last 5 ns was used for production run.

MM/PBSA & ELIE Calculations.

For each system, 50 snapshots evenly extracted from the last 5-ns trajectory were used to calculate the MM/PBSA energy contribution terms (ΔE_{elec}, ΔE_{vdw}, ΔG_{solv_pl}, $\Delta G_{solv-np}$, $T\Delta S$). The water molecules and ions were removed first. The Poisson Boltzmann calculations were performed with the Delphi program [58]. The calculations employed the Parse radii for all atoms, a grid spacing of 0.5 Å, a fill ration of 90%, and a probe radius of

1.4 Å. The value of the exterior dielectric constant was set to 80. The solute interior dielectric constant was set to 1. The nonpolar solvation energy was calculated with the SASA approach, following rescaling using the equation $\Delta G_{nonpol} = \gamma * dSASA + \beta$, where γ=0.00542 kcal/mol/Å^2 and β=0.92 kcal/mol. The NMode module in AMBER16 was applied to derive the entropy loss during protein-ligand binding. After MM/PBSA calculations, the energy contributions in Eq. 3 were extracted using in-house programs and scripts and fed to Eq. 4 for ELIE analysis. The Training Set from literature was used to fit the scaling coefficients in Eq. 4, and then the fitted coefficients were directly applied to the Challenge Set to predict the binding free energies.

Metrics for Analysis

Several measures were used in the coefficient calibrations and posteriori analysis, including mean unsigned error (MUE), root-mean-square error (RMSE), predictive index (PI) [59, 60] and Pearson's r.

The experimental binding free energies were estimated from measured IC50 data [3, 22]:

$$\Delta G_{bind}^{expt} \approx RTln(IC_{50}) \quad (5)$$

Results and Discussion

Pose prediction

The performances of our pose predictions in GC3 are shown in Fig. 1. The submitted prediction with the Glide protocol (submission ID ***rm4m2)*** is displayed in red color, and 3 submissions with the AutoDock Vina protocol are colored in blue. Fig. 1 demonstrates that Glide yielded a much better result than AutoDock Vina. The mean over all pose RMSDs of 24 CatS ligands for our Glide prediction is 3.70 Å (Fig. 1a) and the median over all pose RMSDs is 2.84 A. The mean and median RMSDs for the three predictions with the AutoDock Vina protocols are all approximately 11.0 Å.

The submission ***rm4m2*** contains only one predicted pose for each ligand, and the pose RMSDs for individual ligands are presented in Fig. 2 in red squares. Most of the ligand compounds were docked reasonably well. As a summary 5 ligands have pose RMSDs <= 2.0 Å, 13 ligands have pose RMSDs between 2.0 Å and 4.0 Å, and 6 ligands have pose RMSDs > 4.0 Å. Fig. 3a shows the superposition of predicted pose of CatS-19 to its native pose, which has the lowest RMSD (1.09 Å) in submission ***rm4m2***, and the predicted pose overlays with the native pose very well. Fig. 3b shows CatS-5 which has the largest RMSD (9.89 Å) in ***rm4m2***, and the predicted pose has a flipped orientation comparing to its native pose. CatS-5 is the only etrahydropyrido-pyrazole co-crystallized ligand which does not have a bottom-arm substitution, as shown in Fig. S1 and S2 in the Supplementary Material. Among the high RMSD ligands, CatS-4 & CatS-6 are the only two which do not contain a tetrahydropyrido-pyrazole core but a pyridinone instead (Fig. S1).

The RMSD results for one of the AutoDock Vina predictions (***fibez***) are also presented in Fig. 2. The submission ***fibez*** contains 5 predicted poses for each ligand. The RMSDs of Pose 1 series are displayed with green circles in Fig. 2, and the RMSDs of the Closest Pose series are displayed wtih blue triangles in Fig. 2. Most of the Pose 1 series are not the closest poses for corresponding ligands, and most of them have RMSDs higher than 6.0 Å except for CatS-5 (5.16 Å), CatS-8 (5.66 Å), CatS-12 (4.64 Å), Cats-18 (5.47 Å) and CatS-20 (2.77 Å).

Affinity Prediction by Docking Scores

In ***Stage 1A***, we adopted the scoring functions by Glide and AutoDock Vina to predict the affinity ranking of 136 CatS ligands. The performances of our submissions are shown in Fig. 4. Our Glide prediction ***w83jw*** and one of the Vina prediction ***ppyff*** have comparable performances and both among the top submissions in terms of mean and median Kendall's τ and Spearman's ρ, whereas Glide obviously outperforms Vina in pose predictions aforementioned (Fig. 1).

Affinity Prediction by ELIE

Due to the limited time and computing resource, in ***Stage 1A*** we only managed to complete MD simulations for the Training Set ligands and the 33 ligands in the Free Energy Set with ***3IEJ*** structure as the starting conformation. We fitted the ELIE scale coefficients in Eq. 4 using the Training Set experimental data, and then applied the fitted coefficients to blindly estimate the binding free energies of these 33 ligands in Free Energy Set. As demonstrated in Fig. 5, our submission ***pcy3r*** is at the top place in terms of mean and median correlation coefficients among all submissions to Free Energy prediction in ***Stage 1A.***

In ***Stage 2***, we completed MD simulations for all 136 ligands in the Affinity Ranking Set with the ***3IEJ*** protein structure and estimated their binding free energies with ELIE model. We also took the ***GABJ*** (complex of CatS-14) protein structure and conducted corresponding MD simulations for all the Training Set and Challenge Set and then did the same procedures of coefficient fitting and binding free energy prediction. Fig. 6 shows the retrospective analysis for the intermediate and final results for our submission ***ju2xy*** for ranking prediction in ***Stage 2***.

Fig. 6a & 6c present the MM/PBSA calculated binding free energies for all the Training Set ligands. Comparing to the experimental binding free energies, the MM/PBSA result of ***3IEJ*** series leads to MUE of 2.33 kcal/mol, RMSE of 3.19 kcal/mol, PI of 0.38, Pearson's r of 0.29, and the MM/PBSA result of ***GABJ*** series leads to MUE of 3.37 kcal/mol, RMSE of 4.21 kcal/mol, PI of 0.27 and Pearson's r of 0.22. After applying ELIE method, the ***3IEJ*** series (with coefficients c1=0.9, c2=1.2, c3=1.2, c4=1.0, c5=0.4) leads to MUE of 1.10 kcal/mol, RMSE of 1.32 kcal/mol, PI of 0.54 and Pearson's r of 0.54 (Fig. 6e), and the ***GABJ*** series (with c1=1.1, c2=0.9, c3=1.1, c4=1.3, c5=0.3) leads to MUE of 0.95 kcal/mol, RMSE of 1.15 kcal/mol, PI of 60, and Pearson's r of 0.60 (Fig. 6g). Taking an exponential average of ELIE results of Fig. 6e and Fig. 6g leads to Fig. 6i (MUE = 0.97 Å, RMSE = 1.17 Å, PI = 0.60 and Pearson's r = 0.59).

Similar trend can be found in the results of the Challenge Set. Fig. 6b & 6d present the MM/PBSA calculated binding free energies for all the Challenge Set ligands. Comparing to the experimental binding free energies, the MM/PBSA result of ***3IEJ*** series leads to MUE of 5.70 kcal/mol, RMSE of 7.56 kcal/mol, PI of 0.15, Pearson's r of 0.13, and the MM/PBSA result of ***GABJ*** series leads to MUE of 4.79 kcal/mol, RMSE of 5.86 kcal/mol, PI of 0.20 and Pearson's r of 0.17. After applying ELIE method with the coefficients fitted from the Training Set, the ***3IEJ*** series (with c1=0.9, c2=1.2, c3=1.2, c4=1.0, c5=0.4) leads to MUE of 1.22 kcal/mol, RMSE of 1.64 kcal/mol, PI of 0.40 and Pearson's r of 0.40 (Fig. 6f), and the ***GABJ*** series (with c1=1.1, c2=0.9, c3=1.1, c4=1.3, c5=0.3) leads to MUE of 1.36 kcal/mol, RMSE of 1.89 kcal/mol, PI of 0.35, and Pearson's r of 0.32 (Fig. 6h). Taking an exponential average of ELIE results of Fig. 6f and Fig. 6h leads to Fig. 6j (MUE = 1.32 kcal/mol, RMSE = 1.85 kcal/mol, PI = 0.40 and Pearson's r = 0.38).

The performances of our ELIE protocol for the ranking prediction and the free energy prediction in ***Stage 2*** are displayed in Fig. S3 and S4, respectively. The performances of our submissions (shown in red) are above average in terms of mean and median Kendall's τ and Spearman's ρ. Actually 8 submissions (***m6yb2***, ***e4emg, nmwas, ouj30, fugpp, 3pj6r, e3r6j, pi5ne)*** which are better than or similar to our ***ju2xy*** in Fig. S3, and 11 submissions (***66qqk***, ***tw62k, jk3no, uch2m, rjnyn, vc0p5, feofk, fizwc, 2e2e3, bcfd0***, ***47ka6)*** which are better than or similar to our ***6xwau*** and ***wdgzp*** are from the same participant group with the same method.

Discussion

One common problem and task in real drug design projects is to pre-select which compounds to synthesize and further test with experimental assays which are expensive in terms of both time and cost. Computational methods are expected to be useful in the lead identification and lead optimization stages.

Docking methods have evolved from single rigid receptor conformation – rigid ligand docking to multiple flexible receptor conformations – flexible ligand docking. Even though the state-of-the-art docking protocols are adequate in predicting the correct poses, they are still weak at predicting binding affinities due to the limitations in the scoring functions and ability of sampling. At the same time, alchemical free energy methods like FEP/TI are too computationally demanding to be used routinely for high-throughput screening.

The ELIE method can fill the gap between docking methods and the alchemical free energy methods, so that a more reasonable multi-step workflow can be constructed: firstly docking methods are used to screening millions of compounds for a target and narrow down the number of compounds to thousands or tens of thousands, and then methods like ELIE can be employed to further narrow down the pool of candidates to hundreds or thousands, and then alchemical free energy methods like FEP/TI can kick in to further reduce the candidate quantities to hundreds or tens or even less, before sending to experimentalists. We do not expect the ELIE method to achieve the same accuracy as the rigorous alchemical free energy methods, but we believe that it can be utilized in both lead identification and optimization stages in drug design projects for its balance between efficiency and accuracy.

In D3R GC3 ***Subchallenge 1*** the ELIE method achieved reasonable accuracy for predicting binding free energies comparable to alchemical free energy calculations. Since ELIE is a newly developed method and the participation of this blind challenge is its first application, we think there should exist significant room for further improvement in the future which we plan to explore.

(1) As aforementioned, MD simulations before ELIE analysis in this practice were started from manually generated initial conformations. In order to be suited for routine usage in real drug design projects, initial conformations can be automatically generated from best predicted binding poses by molecular Docking.

(2) For each tautomer/protonation states of each ligand, multiple MD simulations from different initial structures of both receptors and ligands can be carried out to sample more conformational space. And correspondingly, various average algorithms can be explored.

(3) In this challenge, the ELIE coefficients were obtained by coarsely testing. Better fitting algorithms like regressions, gene algorithm, and even machine learning will be explored.

(4) ELIE coefficients need to explicitly trained and calibrated to specific target receptors. The possible common ranges of optimum coefficients for various targets will be searched and verified in the future.

(5) Various conditions that can affect the precision, speed, and accuracy of ELIE results need to be explored, such as the length of MD simulations, etc.

(6) Manual preparation and intervention should be reduced as much as possible and a fully automated pipeline from beginning to end should be set up.

(7) The possibility of merging some of the five energy contribution terms in Eq. 4 can be explored. For example, the ΔE_{elec} and ΔE_{vdw} terms can be merged into one term ΔE_{MM} and share the same coefficient, or the ΔE_{elec} and $d\Delta E_{solv\_pl}$ terms can be merged into one term $d\Delta E_{polar}$ and share one same coefficient, or the ΔE_{vdw} and dE_{solv_np} can be merged into one term $\Delta E_{nonpolar}$ and share one coefficient. By these ways, the five energy contribution terms in Eq. 4 can be merged to four terms to reduce the efforts for coefficient fitting.

(8) The possibility of adopting GBSA continuum solvent model instead of PBSA can be explored.

Conclusion

We developed and utilized the ELIE method when participating in the D3R GC3 in 2017. This is an end-point methodology for calculating binding free energies. It takes snapshots from regular MD simulations of a protein-ligand complex, and then calculates the various energy contributions just like regular MM/PBSA or MM/GBSA. Then we fit the scaling coefficient of energy terms using training set ligands for which the binding affinities were measured, and apply the derived coefficients directly to query ligands of the same receptor target. In principle the ELIE protocol can introduce more accuracy on predictions of protein-ligand binding affinities than simple molecular Docking & Scoring because MD simulations

can imitate the dynamics of protein-ligand interaction in reality. At the same time, it requires much less computing resource and time compared to alchemical free energy calculations.

We thank D3R for the opportunity to test the usefulness of ELIE in a blind challenge which is like a real drug discovery project. The promising performance achieved by ELIE for the CatS subchallenge in GC3 suggests that ELIE could be a good choice for both the lead identification and lead optimization in drug discovery. Our ELIE method is still in the developmental phase and potential improvements have been discussed in this article. We expect a more widespread use of ELIE in prospective drug discovery projects in industry and academia.

Supplementary Material

Refer to Web version on PubMed Central for supplementary material.

Acknowledgements:

This work was supported by the research grants from the National Institutes of Health of USA (R01-GM079383, R21-GM097617, P30 DA035778-01A1). Computational support from the Center for Research Computing of University of Pittsburgh, and the Extreme Science and Engineering Discovery Environment (CHE090098), is acknowledged.

References

1. Drug Design Data Resource. https://drugdesigndata.org. Accessed 25 April 2018.
2. Gathiaka S, Liu S, Chiu M, Yang H, Stuckey JA, Kang YN, Delproposto J, Kubish G, Dunbar JB, Carlson HA, Burley SK, Walters WP, Amaro RE, Feher VA, Gilson MK (2016). D3R grand challenge 2015: Evaluation of protein-ligand pose and affinity predictions. J Comput Aided Mol Des 30:651–668. [PubMed: 27696240]
3. Gaieb Z, Liu S, Gathiaka S, Chiu M, Yang H, Shao C, Feher V, Walters WP, Juhn B, Rudolph MG, Burley SK, Gilson MK, Amaro RE (2018). D3R Grand Challenge 2: blind prediction of protein-ligand poses, affinity rankings, and relative binding free energies. J Comput Aided Mol Des 32:1–20. [PubMed: 29204945]
4. D3R Grand Challenge 3. https://drugdesigndata.org/about/grand-challenge-3. Accessed 25 April 2018.
5. Kramer L, Turk D, Turk B (2017). The Future of Cysteine Cathepsins in Disease Management. Trends Pharmacol Sci 38:873–898. [PubMed: 28668224]
6. Turk V, Stoka V, Vasiljeva O, Renko M, Sun T (2012). Cysteine cathepsins: From structure, function and regulation to new frontiers. Biochim. Biophys Acta 1824:68–88. [PubMed: 22024571]
7. Wiener JJM, Sun S, Thurmond RL (2010). Recent Advances in the Design of Cathepsin S Inhibitors. Curr Top Med Chem 10:717–732. [PubMed: 20337580]
8. Gupta S, Singh RK, Dastidar S, Ray A (2008). Cysteine cathepsin S as an immunomodulatory target: present and future trends. Expert Opin Ther Targets 12:291–299. [PubMed: 18269339]
9. Gustin DJ, Sehon CA, Wei J, Cai H, Meduna SP, Khatuya H, Sun S, Gu Y, Jiang W, Thurmond RL, Karlsson L, Edwards JP (2005). Discovery and SAR studies of a novel series of noncovalent cathepsin S inhibitors. Biorgan Med Chem Lett 15:1687–1691.
10. Ameriks MK, Axe FU, Bembenek SD, Edwards JP, Gu Y, Karlsson L, Randal M, Sun S, Thurmond RL, Zhu J (2009). Pyrazole-based cathepsin S inhibitors with arylalkynes as P1 binding elements. Biorgan Med Chem Lett 19:6131–6134.
11. Ameriks MK, Cai H, Edwards JP, Gebauer D, Gleason E, Gu Y, Karlsson L, Nguyen S, Sun S, Thurmond RL, Zhu J (2009). Pyrazole-based arylalkyne cathepsin S inhibitors. Part II: optimization of cellular potency. Biorgan Med Chem Lett 19:6135–6139.

12. Wiener DK, Lee-Dutra A, Bembenek S, Nguyen S, Thurmond RL, Sun S, Karlsson L, Grice CA, Jones TK, Edwards JP (2010). Thioether acetamides as P3 binding elements for tetradydropyrido-pyrazole cathepsin S inhibitors. Biorgan Med Chem Lett 20:2379–2382.
13. Wiener JJM, Wickboldt AT, Nguyen S, Sun S, Rynberg R, Rizzolio M, Karlsson L, Edwards JP, Grice CA (2013). Pyrazole-based arylalkyne cathepsin S inhibitors. Part III: modification of P4 region. Biorgan Med Chem Lett 23:1070–1074.
14. Ameriks MK, Bembenek SD, Burdett MT, Choong IC, Edwards JP, Gebauer D, Gu Y, Karlsson L, Purkey HE, Staker BL, Sun S, Thurmond RL, Zhu J (2010). Diazinones as P2 replacements for pyrazole-based cathepsin S inhibitors. Biorgan Med Chem Lett 20:4060–4064.
15. Wei J, Pio BA, Cai H, Meduna SP, Sun S, Gu Y, Jiang W, Thurmond RL, Karlsson L, Edwards JP (2007). Pyrazole-based cathepsin S inhibitors with improved cellular potency. Biorgan. Med Chem Lett 17:5525–5528.
16. Pauly TA, Sulea T, Ammirati M, et al. (2003) Specificity Determinants of Human Cathepsin S Revealed by Crystal Structures of Complexes. Biochemistry (Mosc) 42:3203–3213.
17. Markt P, McGoohan C, Walker B, et al. (2008) Discovery of Novel Cathepsin S Inhibitors by Pharmacophore-Based Virtual High-Throughput Screening. J Chem Inf Model 48:1693–1705. [PubMed: 18637674]
18. Thurmond RL, Sun S, Sehon CA, et al. (2004) Identification of a Potent and Selective Noncovalent Cathepsin S Inhibitor. J Pharmacol Exp Ther 308:268–276. [PubMed: 14566006]
19. D3R Grand Challenge 3 Evaluation Results. https://drugdesigndata.org/about/grand-challenge-3-evaluation-results. Accessed 20 April 2018.
20. Zwanzig RW (1954) High-temperature equation of state by a perturbation method. I. nonpolar gases. J Chem Phys 22:1420–1426.
21. Kirkwood JG (1935) Statistical mechanics of fluid mixtures. J Chem Phys 3:300–313.
22. Wang L, Wu Y, Deng Y, Kim B, Pierce L, Krilov G, Lupyan D, Robinson S, Dahlgren M, Greenwood J, Romero DL, Masse C, Knight JL, Steinbrecher T, Beuming T, Damm W, Harder E, Sherman W, Brewer M, Wester R, Murcko M, Frye L, Farid R, Lin T, Mobley DL, Jorgensen WL, Berne BJ, Friesner RA, Abel R (2015) Accurate and reliable prediction of relative ligand binding potency in prospective drug discovery by way of a modern free-energy calculation protocol and force field. J Am Chem Soc 137:2695–2703. [PubMed: 25625324]
23. Hu Y, Sherborne B, Lee T-S, Case DA, York DM, Guo Z (2016) J Comput Aided Mol Des 30(7): 533–539. [PubMed: 27480697]
24. Mobley DL, Gilson MK (2017). Predicting binding free energies: frontiers and benchmarks. Annu Rev Biophys 46:531–558. [PubMed: 28399632]
25. Gilson MK, Zhou HX (2007). Calculation of protein-ligand binding affinities. Annu Rev Biophys Biomol Struct. 36:21–42. [PubMed: 17201676]
26. Aqvist J, Medina C, Samuelsson JE (1994) A new method for predicting binding affinity in computer-aided drug design. Protein Eng 7:385–391. [PubMed: 8177887]
27. Hansson T, Marelius J, Aqvist J (1998) Ligand binding affinity prediction by linear interaction energy methods. J Comput Aided Mol Des 12:27–35. [PubMed: 9570087]
28. Vosmeer CR, Pool R, Van Stee MF, Perić-Hassler L, Vermeulen NPE, Geerke DP (2014) Towards automated binding affinity prediction using an iterative linear interaction energy approach. Int JMol Sci 15:798–816. [PubMed: 24413750]
29. Capoferri L, Verkade-Vreeker MCA, Buitenhuis D, Commandeur JNM, Pastor M, Vermeulen NPE, Geerke DP (2015) Linear interaction energy based prediction of cytochrome P450 1A2 binding affinities with reliability estimation. PLoS ONE 10:1–23.
30. Srinivasan J, Cheatham TE, Cieplak P et al. (1998) Continuum solvent studies of the stability of DNA, RNA, and phosphoramidate-DNA helices. J Am Chem Soc 120:9401–9409.
31. Hou T, Wang J, Li Y, Wang W (2011) Assessing the performance of the MM/PBSA and MM/GBSA methods. 1. The accuracy of binding free energy Calculations based on molecular dynamics simulations. J Chem Inf Model 51:69–82. [PubMed: 21117705]
32. Genheden S, Ryde U (2015) The MM/PBSA and MM/GBSA methods to estimate ligandbinding affinities. Expert Opin Drug Discov 10:449–461. [PubMed: 25835573]

33. Berman HM, Westbrook J, Feng Z, Gilliland G, Bhat TN, Weissig H, Shindyalov IN, Bourne PE (2000) The protein data bank. Nucleic Acids Res 28:235–242. [PubMed: 10592235]
34. Sastry GM, Adzhigirey M, Day T, Annabhimoju R, Sherman W (2013) Protein and ligand preparation: parameters, protocols, and influence on virtual screening enrichments. J Comput Aided Mol Des 27:221–234. [PubMed: 23579614]
35. Schrödinger LLC (2017) Schrödinger Release 2017-2: Maestro, Schrodinger LLC, New York, NY.
36. Jacobson MP, Friesner RA, Xiang Z, Honig B (2002) On the Role of Crystal Packing Forces in Determining Protein Sidechain Conformations. J Mol Biol 320:597–608. [PubMed: 12096912]
37. Shelley JC, Cholleti A, Frye L, Greenwood JR, Timlin MR, Uchimaya M (2007) Epik: a software program for pK_a prediction and protonation state generation for drug-like molecules. J Comput Aided Mol Des 21:681–691. [PubMed: 17899391]
38. Harder E, Damm W, Maple J, Wu C, Reboul M, Xiang JY, Wang L, Lupyan D, Dahlgren MK, Knight JL, Kaus JW, Cerutti DS, Krilov G, Jorgensen WL, Abel R, Friesner RA (2015) OPLS3: A Force Field Providing Broad Coverage of Drug-like Small Molecules and Proteins. J Chem Theory Comput 12:281–296. [PubMed: 26584231]
39. Friesner RA, Banks JL, Murphy RB, Halgren TA, Klicic JJ, Mainz DT, Repasky MP, Knoll EH, Shaw DE, Shelley M, Perry JK, Francis P, Shenkin PS (2004) Glide: A New Approach for Rapid, Accurate Docking and Scoring. 1. Method and Assessment of Docking Accuracy. J Med Chem 47:1739–1749. [PubMed: 15027865]
40. Friesner RA, Murphy RB, Repasky MP, Frye LL, Greenwood JR, Halgren TA, Sanschagrin PC, Mainz DT (2006) Extra Precision Glide: Docking and Scoring Incorporating a Model of Hydrophobic Enclosure for Protein-Ligand Complexes. J Med Chem 49:6177–6196. [PubMed: 17034125]
41. Trott O, Olson AJ (2010) AutoDock Vina: improving the speed and accuracy of docking with a new scoring function, efficient optimization, and multithreading. J Comput Chem 31:455–461. [PubMed: 19499576]
42. Sanner MF (1999). Python: A Programming Language for Software Integration and Development. J Mol Graphics Model 17:57–61.
43. Wang J, Wang W, Kollman PA, Case DA (2006) Automatic atom type and bond type perception in molecular mechanical calculations. J Mol Graph Model 25:247–260. [PubMed: 16458552]
44. Wang J, Wolf RM, Caldwell JW et al. (2004) Development and testing of a general amber force field. J Comput Chem 25:1157–1174. [PubMed: 15116359]
45. Jakalian A, Bush BL, Jack DB, Bayly Cl (2000) Fast, efficient generation of high-quality atomic charges. AM1-BCC model: I Method. J Comput Chem 21:132–146.
46. Cl Bayly, Cieplak P, Cornell W, Kollman PA (1993). A Well-Behaved Electrostatic Potential Based Method Using Charge Restraints for Deriving Atomic Charges: The RESP Model. J Phys Chem 97:10269–10280.
47. Gaussian 16, Revision A.03, Frisch MJ, Trucks GW, Schlegel HB, Scuseria GE, et al. (2016) Gaussian, Inc., Wallingford CT.
48. Maier JA, Martinez C, Kasavajhala K, Wickstrom L, Hauser KE, Simmerling C (2015) ff14SB: Improving the Accuracy of Protein Side Chain and Backbone Parameters from ff99SB. J Chem Theory Comput 11:3696–3713. [PubMed: 26574453]
49. Jorgensen WL, Chandrasekhar J, Madura JD, Impey RW, Klein ML (1983) Comparison of Simple Potential Functions for Simulating Liquid Water. J Chem Phys 79:926–935.
50. Case DA, Betz RM, Cerutti DS, et al. (2016) AMBER 2016, University of California, San Francisco.
51. Goetz AW, Williamson MJ, Xu D, Poole D, Grand SL, Walker RC (2012) Routine microsecond molecular dynamics simulations with AMBER - Part I: Generalized Born. J Chem Theory Comput 8:1542–1555. [PubMed: 22582031]
52. Salomon-Ferrer R, Goetz AW, Poole D, Grand SL, and Walker RC (2013) Routine microsecond molecular dynamics simulations with AMBER - Part II: Particle Mesh Ewald. J Chem Theory Comput 9:3878–3888. [PubMed: 26592383]

53. Loncharich RJ, Brooks BR, Pastor RW (1992) Langevin dynamics of peptides: The frictional dependence of isomerization rates of N-acetylalanyl-N'-methylamide. Biopolymers 32:523–535. [PubMed: 1515543]
54. Izaguirre J, Catarello D, Wozniak J, Skeel R (2001) Langevin stabilization of molecular dynamics. J ChemPhys 114:2090–2098.
55. Darden T, York D, Pedersen L (1993) Particle Mesh Ewald: An N.Log (N) Method for Ewald Sums in Large Systems. J Chem Phys 98:10089–10092.
56. Essmann U, Perera L, Berkowitz ML (1995) A smooth particle mesh Ewald method. J Chem Phys 103:8577–8593.
57. Ryckaert JP, Ciccotti G, Berendsen HJC (1977) Numerical Integration of the Cartesian Equations of Motion of a System with Constraints: Molecular Dynamics of N-Alkanes. J Comput Phys 23:327–341.
58. Rocchia W, Alexov E, Honig B (2001). Extending the applicability of the nonlinear Poisson-Boltzmann equation: multiple dielectric constants and multivalent ions. J Phys Chem B 105:6507–6514.
59. Pearlman DA, Charifson PS (2001). Are free energy calculations useful in practice? A comparision with rapid scoring functions for the p38 MAP kinase protein system. J. Med. Chem. 44:3417–3423. [PubMed: 11585447]
60. Luccarelli J, Michel J, Tirado-Rives J, Jorgensen WL (2010). Effects of water placement on predictions of binding affinities for p38α MAP kinase inhibitors. J. Chem. Theory Comput. 6:3850–3856. [PubMed: 21278915]
61. The evaluation results for the pose prediction of Cathepsin Stage 1A. https://drugdesigndata.org/php/d3r/gc3/combined/pose/index.php?component=968&results=rmsd&chart=pose&partial=0&ligand=Mean. Accessed 20 April 2018.
62. The evaluation results for the Ranking Set of Cathepsin Stage 1A. https://drugdesigndata.org/php/d3r/gc3/combined/scoring/index.php?component=968&method=ligand&partial=0&group=noties. Accessed 20 April 2018.
63. The evaluation results for the Free Energy Set of Cathepsin Stage 1A. https://drugdesigndata.org/php/d3r/gc3/combined/free-energy/index.php?component=968&partial=0&group=noties. Accessed 20 April 2018.

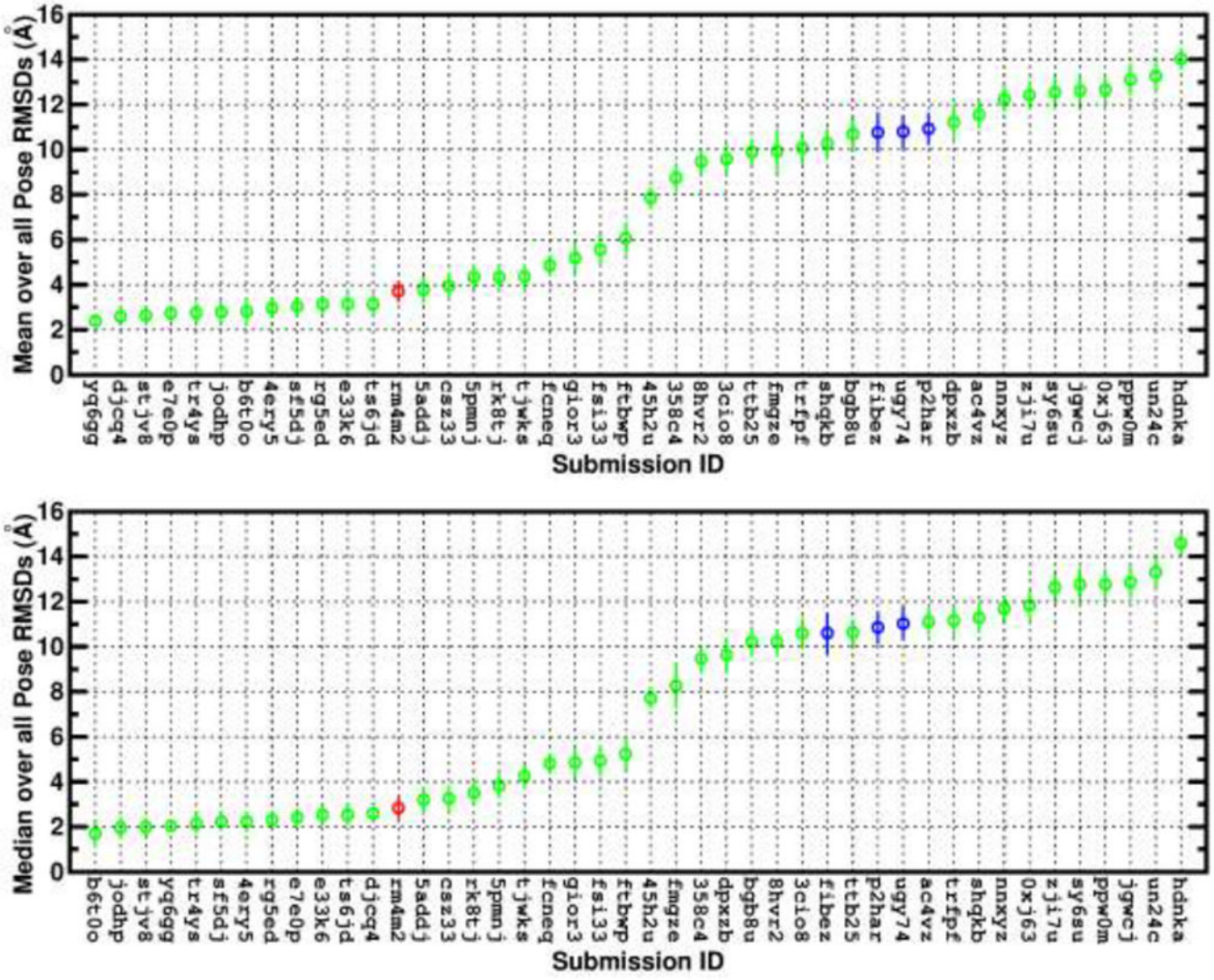

Fig. 1.

Performance of all pose prediction submissions in GC3 Subchallenge 1 analyzed by pose RMSDs from Pose 1 of all submissions: mean RMSD over all 24 ligands (upper panel), and median RMSD over all 24 ligands (lower panel). Our submission by Glide protocol is displayed in red, and our submissions by AutoDock Vina are displayed in blue. The error bars show the standard error which is equal to the standard deviation (STD) divided by the square root of sample size (24). The data of median, mean and STD RMSDs were evaluated by the challenge organizers [61].

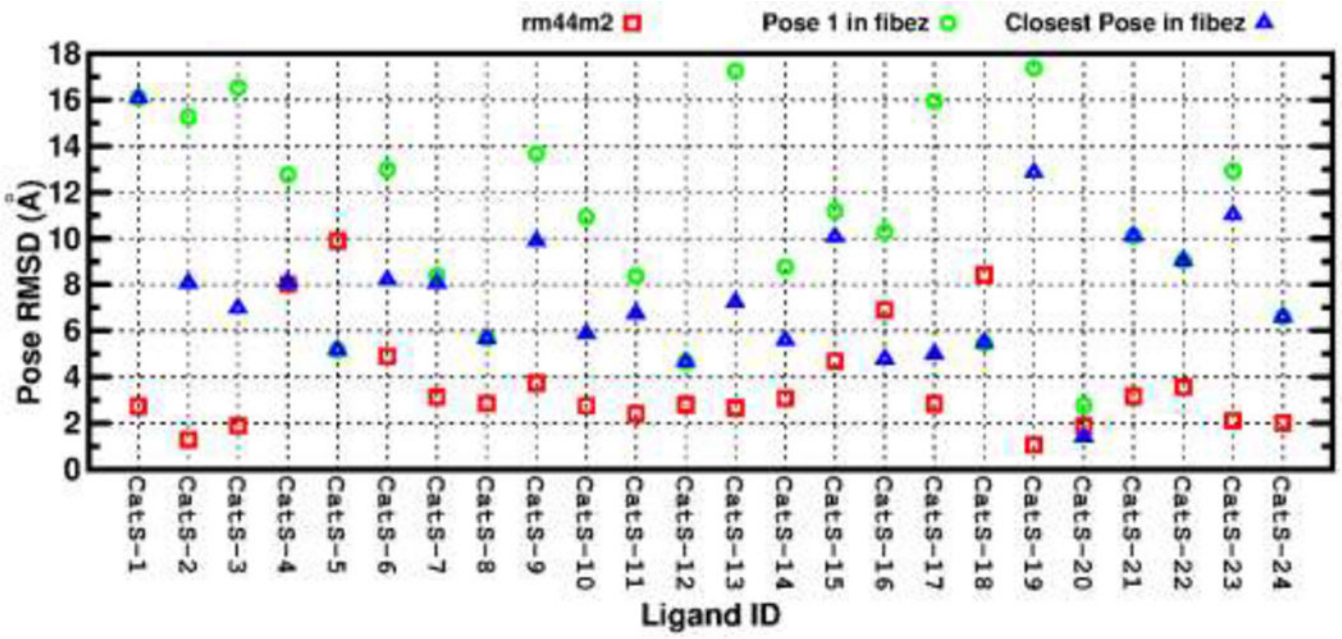

Fig. 2.

The pose RMSDs for 24 CatS ligands of our predictions ***rm4m2*** (Glide XP) and ***fibez*** (AutoDock Vina) comparing to the corresponding crystal structures. The submission ***rm4m2*** contains only 1 pose for each ligand, and corresponding RMSDs for individual ligands are shown with red squares. The submission ***fibez*** contains 5 poses for each ligand, and corresponding RMSDs of Pose 1 series are shown with green circles, and the RMSDs of the Closest Pose series are shown wtih blue triangles.

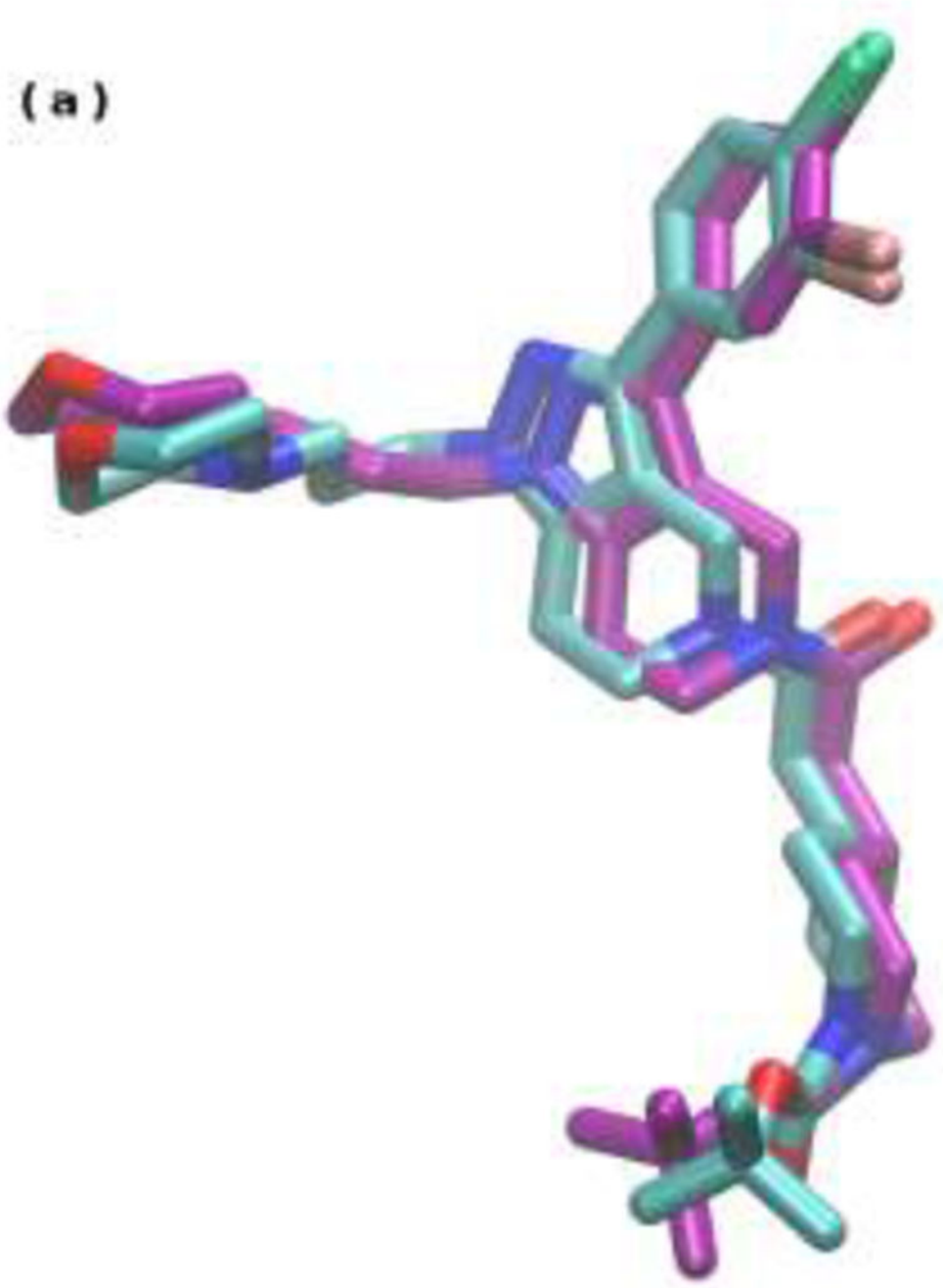

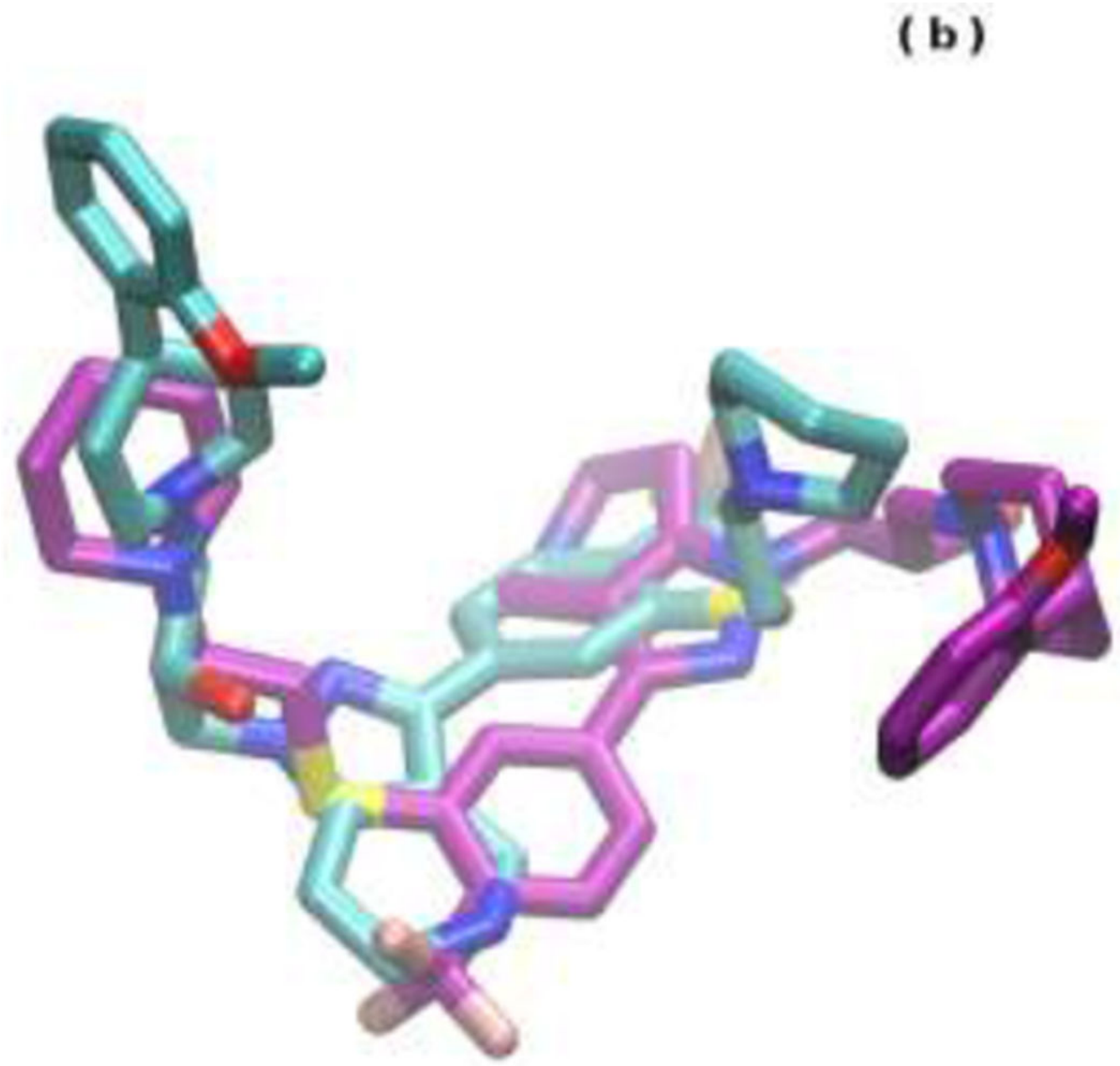

Fig. 3.

Superposition of the predicted binding poses (submission ID ***rm4m2***, shown in purple) on the native crystallized poses (C in cyan, N in blue and O in red) for CatS-19 (RMSD = 1.09 Å, left) and CatS-5 (RMSD = 9.89 Å, right).

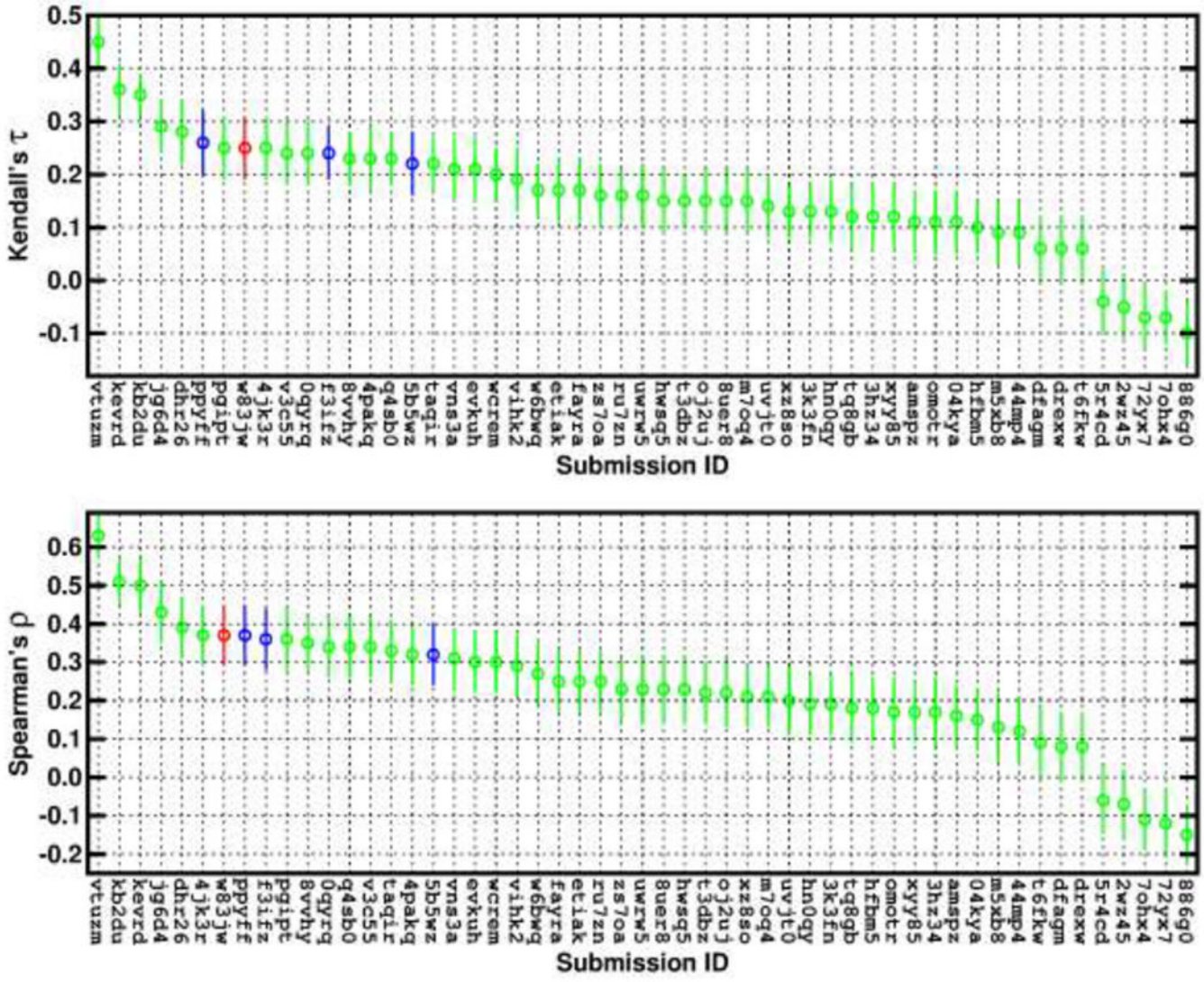

Fig. 4.

Performance of our ranking predictions in Stage 1A of GC3 Subchallenge 1. Our submission by Glide scoring is displayed in red, and our submissions by AutoDock Vina scoring are displayed in blue. The evaluation data were provided by the challenge organizers [62].

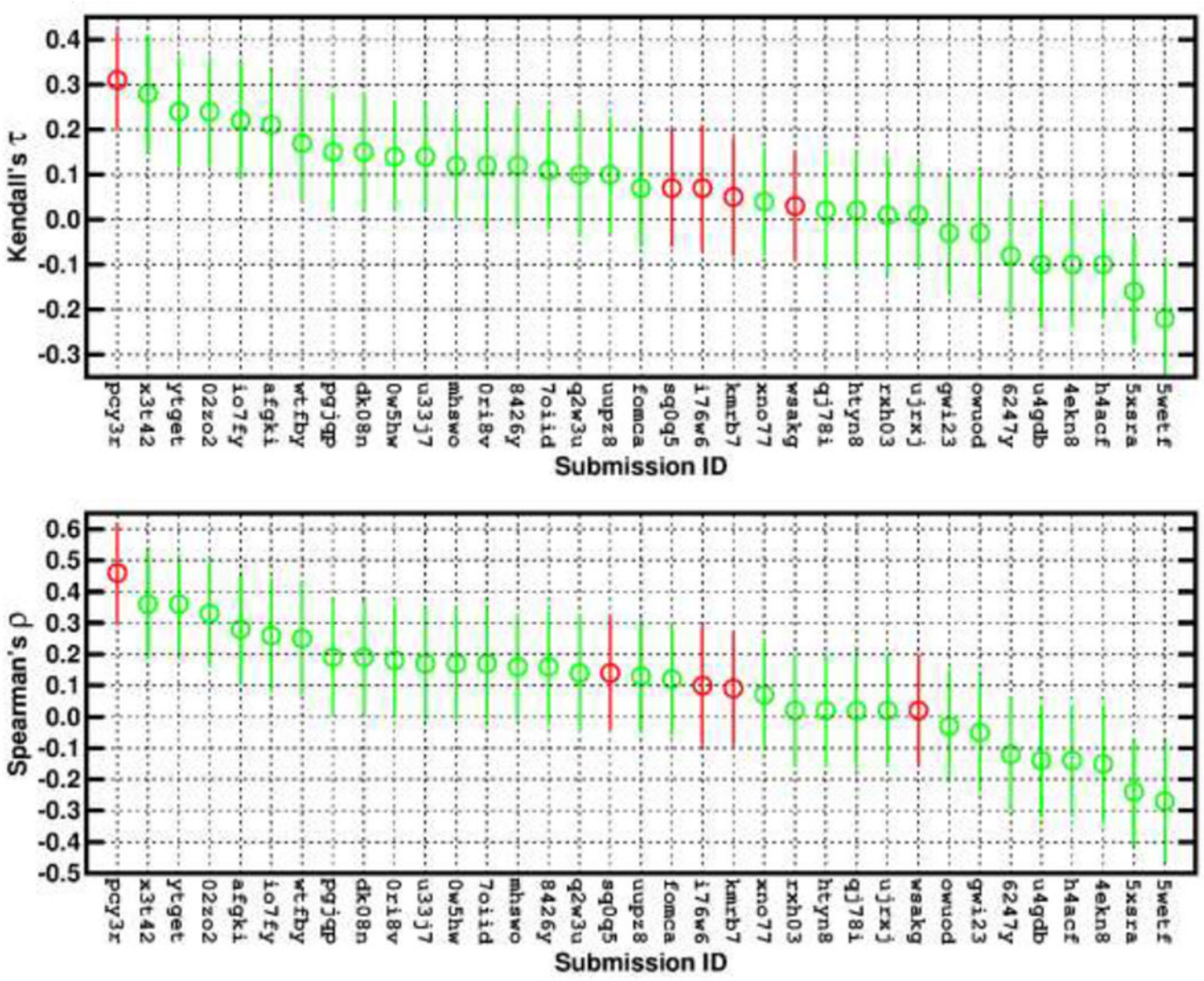

Fig. 5.

Performance of predictions for the CatS Free Energy set in Stage 1 A. Our predictions with ELIE methods are displayed in red color. The evaluation data were provided by the challenge organizers [63].

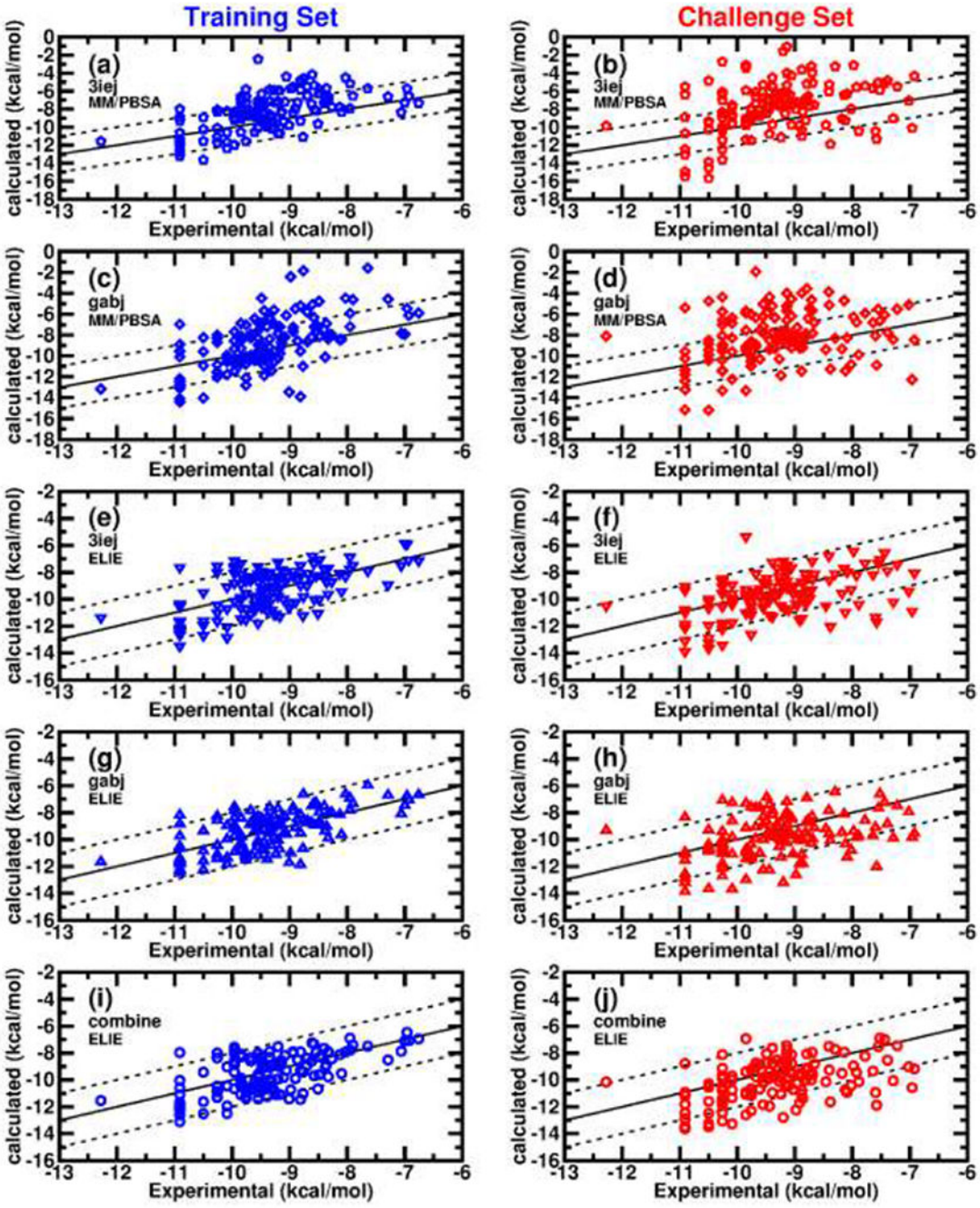

Fig. 6.

Estimation of binding free energies for the Training Set (a, c, e, g, i) and Challenge Set (b, d, f, h, j). The calculation method is either MM/PBSA or ELIE as shown in the label of each panel. The initial protein structure is either ***3iej*** or ***gabj*** as indicated by the labels of a to h, and "combine" by the labels of i & j stands for taking averages from the results of ***3iej*** and ***gabj*** series as described in the main text.